2013 IEEE/RSJ International Conference on
Intelligent Robots and Systems (IROS)
November 3-7, 2013. Tokyo, Japan

Modeling and identification of the human arm stretch reflex using a realistic spiking neural network and musculoskeletal model

Manish Sreenivasa, Akihiko Murai, and Yoshihiko Nakamura

***Abstract*— This study proposes a model that combines a realistically scaled neural network made up of pools of spiking neurons, with a musculoskeletal model of the human arm. We used evidence from literature to design topological pools of spinal neurons and their synaptic connections. The spiking output of the motor neuron pools were used as the command signals that generated motor unit forces, and drove joint motion. Feedback information from muscle spindles was relayed to the neural network via monosynaptic and disynaptic pathways. Participant-specific parameters of the combined neuromusculoskeletal (NMS) system were then identified from recorded experimental data. The identified NMS model was used to simulate the arm stretch reflex and the results were validated by comparison to an independent recorded dataset. The models and methodology proposed in this study show that large and complex neural systems can be identified in conjunction with the musculoskeletal systems that they control. This additional layer of detail in NMS models has important relevance to the research communities related to rehabilitation robotics and human movement analysis.**

I. MOTIVATION

Modeling of human neuromuscular physiology plays a vital role in furthering our understanding of normal and pathological movements. A class of such models incorporate methods used in robotics such as kinematics, dynamics, optimization and mathematical modeling to simulate physical movements as the result of interactions between the neural, muscular and skeletal systems [1], [2], [3], [4]. Among the biggest challenges in neuromusculoskeletal (NMS) modeling are 1) Approximating complex neuromuscular behavior by mathematical functions that are reasonably simple, and 2) Determining parameters for these functions that can accurately reproduce behavior outside of those directly recorded. The Central Nervous System (CNS) organizes movements by a tight coupling of action, feedback and reaction with the muscular and skeletal systems. Despite this, it is possible to isolate and study parts of this large complex system. For example, the work on motor control and reinforcement learning by Doya et al. [5] focuses on the planning and modulation of movements from a neural perspective, by modeling large populations of neurons and studying the emergent behavior from interactions between neurons. From a more physical perspective, we can also consider the body as a biomechanical device interacting dynamically or passively with the environment. Studies can then focus on the actuation of this rigid-body skeletal structure with muscles modeled as wires [2], [1] or finite element deformable volumes [6]. Studies that combine neural control signals with musculoskeletal models have the advantage of being closer to the biological process, but can become computationally infeasible due to large model scales. By reducing the complex neural dynamics to simpler functions of lesser dimensions, we can focus on a subset of movements occurring via known physiological processes (for example, [2], [3]). These models have the ability to capture some of the macroscopic movement behaviors such as disturbance compensation [7], [8], stable locomotion [7] and the stretch reflex [4]. However, as a limitation of the simplified control architecture, subtle aspects of movement generation such as the recruitment principle and rate coding [9], may be difficult to capture.

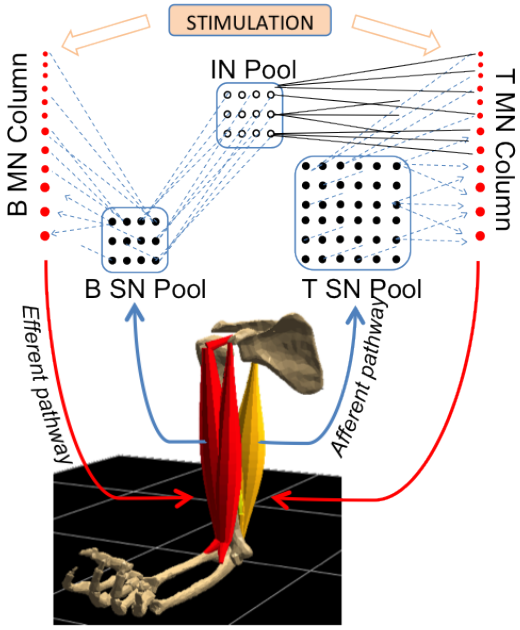

Fig. 1. Schematic of the stretch reflex mechanism: In the posture illustrated above, a stretch in the bicep muscle spindles causes the corresponding sensory neurons (B SN) to fire. This causes subsequent excitation of the Bicep motor neurons (B MN) via a monosynaptic pathway (B SN $>$ B MN), and simultaneous inhibition of the tricep motor neurons (T MN) via a disynaptic pathway (B SN $>$ IN $>$ T MN). Note that only some of the synaptic connections are shown for clarity of illustration.

Contributions:
This study models the stretch reflex of the bicep muscle in the posture illustrated in Fig. 1. The model components are detailed in Section II, followed by the human experiments (Section III) used in the model parameter identification process, Section IV. Results are presented in Section V and

Department of Mechano-Informatics, University of Tokyo, 7-3-1 Hongo, Bunkyo-ku, Tokyo 1138656, Japan manu/murai/nakamura at ynl.t.u-tokyo.ac.jp

discussed in Section VI. The following contributions arise from this study:

- Integration of realistic "spiking" neural networks with musculoskeletal models
- Development of experimental and parameter estimation methods for combined NMS models
- Simulation of the bicep stretch reflex in the human arm

II. NEUROMUSCULOSKELETAL MODEL

Fig. 1 shows an overview of the NMS model used in this study. The network architecture and neuron model equations detailed in this section were implemented in the software NEST [10]. Forward kinematics and forward dynamics were simulated using a custom-built software using robotics algorithms and musculo-skeletal visualization, sDIMS [1]. Communication between the NEST and sDIMS simulators was implemented in the Message Parsing Interface (MPI) parallel computing environment, using the MUSIC framework [11].

A. Neural Network

The neural network consisted of topological distributions of Motor Neurons (MN), Sensory Neurons (SN) and InterNeurons (IN). The control input to the neural network was constant stimulation (simulated DC current) applied directly to the MN pools, and represented the cumulative descending drives coming from the upper motor neurons and higher brain centers.

Motor Neurons (MN): In biological muscle, one MN can enervate several hundreds of muscle fibres; this is termed as a *Motor Unit (MU)*. For our study we chose the average number of MUs found in the bicep, $N_B = 120$, and tricep, $N_T = 240$, muscles based on counts from human physiology [12]. It is also known that MUs are of varying strengths, and that weaker MUs are slower and controlled by smaller MNs (and vice versa). This type of architecture encodes the *recruitment principle* [9], which states that for a given recruitment (force) level, smaller MNs fire before larger ones. To model this change in MN size, we varied the membrane capacitance as smaller neurons have lower capacitance and hence fire first. Human spinal MN diameters are known to vary from 50μm to 90μm [9]. According to [13], specific membrane capacitance of spinal cord neurons in the rat ventral horn have been found to be 1.5 to 2.28μF/cm^2. Assuming a spherical surface area of the neuron, we then get a variation for membrane capacitance from 117pF to 580pF. This variation was reproduced as a linearly increasing function of MN count (1 = smallest, N = largest); $C_i = C_{SF}(N/2-i)+r_c$, with C_i as the membrane capacitance of the i_{th} MN, r_c a constant that determines the mid-point of the distribution (defined in Table II-A), N the total number of MNs (in that specific pool), and C_{SF} the scaling factor used in parameter identification (detailed later in Sec. IV). Dynamic behavior of MNs was modeled using the *Integrate And Fire* (IAF) neuron model [14]. The IAF model represents the general electrical behavior of neurons as:

$$\frac{dV_m}{dt} = -\left(\frac{V_m - E_L}{\tau_m}\right) + \frac{I_{syn}(t)}{C} + \frac{I_e}{C} \qquad (1)$$

where V_m is the membrane potential, E_L is the resting membrane potential, τ_m is the membrane time constant, $I_{syn}(t)$ is the sum of alpha-shaped synaptic currents, I_e is the constant external input current and C the membrane capacitance. Note that in our study we only modify the capacitance C and assume default values estimated from physiology for the other parameters (listed in Table II-A). Details of the neuron model and integration scheme for the subthreshold dynamics can be found in [14].

Neuromuscular Junction: Based on the MN pools modeled above, the output of the neural network was $(N_B + N_T)$ efferent channels containing spike events. In human physiology, these spikes result in MU twitch forces via electrochemical processes occurring at the junction of the MN axons and the muscle fibres, called the *motor end plates*. We decomposed this process into two parts: 1) neural spike to activation 2) activation to MU force. The latter part is detailed in Section II-B. Neural spike to activation was approximated as the impulse response of a second-order system [15]. In our implementation we used a modified version of the discrete time equations developed by Cisi & Kohn [3]:

$$a(t) = 2\exp\left(\frac{t}{Tmax}\right)a(t-1) - \exp\left(\frac{-2t}{Tmax}\right)a(t-2) + \frac{t^2}{Tmax}\exp\left(1-\frac{t}{Tmax}\right)u(t) \qquad (2)$$

$$\text{with, } u(t) = \begin{cases} 1, \text{ if spike detected} \\ 0, \text{ if no spike detected} \end{cases} \qquad (3)$$

where, $a(t)$ was the activation at time instance t and $Tmax$ the time to maximum force. Note that eq. (2) gives us the instantaneous activation level of one MU (associated with spiking behavior of one MN).

Sensory Neurons (SN): Each muscle spindle (MS) in the muscle body is associated with one SN located just outside the central spinal pools. Note that we henceforth use the terms MS and SN interchangeably as they represent the same physiological entity. The focus of this study was related to the quickest of the MS pathways, the *1a afferent*, with a response time of about 20-30ms and primarily responsible for encoding muscle velocity information. In a comparison of various spindle models, Prochazka et al. [16] commented on the efficiency of simple power-law models in representing the macroscopic firing characteristics of cat muscle spindles. Here, we were interested in only the first term of this model that encodes the 1a afferent response, $f(t) = 4.3v(t)^{0.6}$. Frequency of spindle spikes $f(t)$ was calculated from muscle velocities $v(t)$ in the forward dynamics simulation. We then used a poisson process (as implemented in NEST [10]) to approximate the frequency $f(t)$ by discrete spike events. We uniformly distributed, $N_{BMS} = 52$, spindles in the bicep muscle and, $N_{TMS} = 102$, in the tricep muscle, based on spindle counts from physiological studies [17].

Topology & Synaptic Connections: The neuron pools shown in Fig. 1 were organized topologically to mirror their arrangement in the human spine. This is especially important as synaptic strengths were decided by the relative distance.

Delay due to signal transmission (axonal conduction time), was fixed at 5ms from MN to motor end plate and from MS to SN, and 2ms for all other connections between neuron pools. MNs of the bicep and tricep were arranged in vertical columns, with each neuron a unit distance apart. SN pools were arranged in a square grid, such that the grid centers matched those of their respective MN columns. The relative distances between the pools were chosen such that they approximated the dimensions of their arrangement in the human spinal column. The IN pool was arranged in a square grid of $N_I = 50$ identical IAF neurons located between the two SN pools (IN default parameters are listed in Table II-A). The number of IN in the pool, N_I, was chosen such that it approximates the IN/MN ratio found in the human spine [9]. Note that here we only model the IN pool responsible for inhibition of the tricep muscle (as antagonist). Two types of pathways connected the various neuron pools as shown in Fig. 1; 1) Monosynaptic Agonist Excitation and 2) Disynaptic Antagonist Inhibition. For all pathways, we assumed that all source neurons connect to all target neurons. The synaptic weight of the connection was varied according to the distance between each source-target pair. The exact values of synaptic weights in physiology is difficult to determine, however, it is well known that neurons closest to each other form the strongest synapses and that this synaptic weight rapidly decreases with distance between pairs [9]. Here, we modeled this phenomenon as a symmetrical Gaussian distribution with magnitude w and variance σ, as a function of the distance between connecting pairs. Thus, for our network all synaptic values could be determined from the parameters:

- w_{BB+} & σ_{BB+}: Maximum weight and variance of synaptic distribution for Bicep SN to Bicep MN connections, the '+' denotes excitation
- w_{TT+} & σ_{TT+}: Synaptic properties for Tricep SN to Tricep MN
- w_{BI+} & σ_{BI+}: Synaptic properties for Bicep SN to IN
- w_{IT-} & σ_{IT-}: Synaptic properties for IN to Tricep MN, the '-' denotes inhibition

B. Musculoskeletal Model

The network detailed above is applicable to any generic arrangement of agonist-antagonist muscle pair. In this study we focus on the biceps and triceps muscles. This choice was motivated by the large amount of literature available on the neurophysiology of the arm muscles, and, the relative ease of recording experimental data on the human arm (compared to leg muscles). We also note that the bicep stretch reflex is an important neural mechanism from a clinical perspective and is commonly used to test for neurological pathology. The arm was modeled as 2 rigid bodies, a fixed upper arm (including shoulder) and forearm (including hand), connected by a rotational joint at the elbow, Fig. 1. The skeletal bones were scaled to the participant-specific dimensions by using the marker data collected during experiments. Musculoskeletal mass and inertia properties were approximated from participant proportions and anthropometric data [1]. The elbow joint was actuated by means of massless wires, representing the bicep and tricep muscles. Insertion points and muscle line-of-action were chosen carefully based on anatomical literature. MU activations (eq. (2)) were used to calculate MU twitch forces, and a summation of all MU twitches at a time instant gave the total muscle force. Activation to twitch force was computed using the Hill-type muscle model equation $F(t) = a(t)f(l)f(v)Fmax$, which relates muscle force $F(t)$ to the instantaneous activation level $a(t)$, muscle length $f(l)$, velocity $f(v)$ and maximum tetanic force $Fmax$. In this study, $Fmax$ was a distribution over $N_B + N_T$ MUs for each muscle. Additionally, we recall that the dynamic behavior of each MU was affected by the time to maximum force, $Tmax$ eq. (2). The relation between the MU maximum force and time to maximum force was modeled according to the distribution:

$$Fmax_i = \left[p_f log(N-i) + r_f\right] Fmax_{SF} \quad (4)$$

$$Tmax_i = \left[e^{p_t Fmax_i} + r_t\right] Tmax_{SF} \quad (5)$$

where, $Fmax_i$ and $Tmax_i$ are the maximum force and time to peak force of the i_{th} MU, respectively. $Fmax_{SF}$ and $Tmax_{SF}$ are scaling factors that determine the parameters of individual MUs. p_f, p_t, r_f and r_t are constants that determine the shape of the distribution (defined in Table II-A). Eq. (4) and (5) model MUs similar to that found in physiological muscle, and are often referred to as S (Slow), FF (Fast Fatigue) and FR (Fatigue Resistant) muscle fibres in biomechanical studies. Additionally, resistance from synovial fluid (viscous fluid between moving bony surfaces), was modeled as a resistive torque, τ^-, proportional to the joint velocity, $\dot{q}$; $\tau^- = \dot{q}\tau_{SF}$, where, the scaling factor τ_{SF} was to be determined in the identification process.

III. EXPERIMENTS

Two experiments were designed to independently identify steady-state and dynamic parameters of the NMS model. The methodology employed in these experiments were similar to those used by Schouten et al. [4] to study proprioceptive feedback in the human shoulder. Participant joint position data were collected using a motion capture system (Motion-Analysis Co., USA) by attaching 8 markers to the shoulder, upper arm, forearm and wrist. 3 wireless Electromyographs (EMG) were attached to the skin by palpitating the mid-point of the biceps muscle, and the lateral and medial heads of the triceps muscle. For the first experiment, we also used a bi-directional force sensor (Imada Z2-1 J, Range $\pm$500N, Resolution 0.001N), that was firmly attached to the wrist by means of a cushioning band and a rigid metal strap. The sensor was mounted on a heavy pedestal such that it could not be moved by the participant during the trial. Marker positions, EMG signals and force sensor data were recorded at time-matched instances at 200Hz.

In experiment 1, "Graded Recruitment" (GR), the participant was asked to position the forearm horizontally while keeping the upper arm vertical. The force sensor was positioned such that sensor axis was directly below the participant's wrist. The wrist band and metal strap were attached such that a downward or upward force could

Component	No. of Components	Fixed Parameters/Behavior	Biological/Identification Search Range	**Model Identified Values**
Bicep MN	120	$E_L = V_m = -70$mV	117pF $\leq C_B \leq$ 580 pF	156pF $\leq C_B \leq$ 541pF
Tricep MN	240	$\tau_m = 10$ms, $V_{th} = -55$mV $r_c = 348.5$	117pF $\leq C_T \leq$ 580pF	61pF $\leq C_T \leq$ 535pF
Interneurons	50	$E_L = V_m = -70$mV, $\tau_m = 10$ms $V_{th} = -55$mV, $C = 160$pF	-	-
Bicep MU Maximum Twitch Force	120	$p_f = -0.2232, r_f = 1.28$ Eq. (4)	3.25N $\leq Fmax_B \leq$ 44.76N	6.71N $\leq Fmax_B \leq$ 23.07N
Tricep MU Maximum Twitch Force	240		3.25N $\leq Fmax_T \leq$ 44.76N	4.22N $\leq Fmax_T \leq$ 18.18N
Bicep MU Time to Maximum Force	120	$p_{tb} = -0.4, r_{tb} = 0.04$ Eq. (5)	32ms $\leq Tmax_B \leq$ 132ms	41ms $\leq Tmax_B \leq$ 112ms
Tricep MU Time to Maximum Force	240	$p_{tt} = -1.45, r_{tt} = 0.04$ Eq. (5)	32ms $\leq Tmax_T \leq$ 132ms	41ms $\leq Tmax_B \leq$ 115ms
Synovial (resistive) torque	-	-	-0.3 $\leq \tau_{SF} \leq$ -0.01	τ_{SF}=-0.1114
Identified Synaptic Parameters: $w_{BB+} = 53.04, \sigma_{BB+} = 3.32$ $w_{TT+} = 25.31, \sigma_{TT+} = 8.25$ $w_{BI+} = 148.91, \sigma_{BI+} = 103.31$ $w_{IT-} = -43.37, \sigma_{IT-} = 13.08$				

be exerted on sensor by extending or flexing the elbow, respectively. Over a course of 11 conditions, the participant was asked exert forces from -50N (pushing downwards) to +50N (pulling upwards) in steps of 10N. Conditions were presented in randomized order. During each condition the participant could see a display of the current force being exerted on the force sensor. Once the prescribed force level was achieved, the participant was asked to maintain it for 10 seconds. In experiment 2, "Co-contracted Reflex" (CR), we followed a 3 arm position (extended, horizontal, flexed) $\times$ 3 co-contraction level (low, medium, high) design. At each of these combinations, we applied a sudden perturbation to the wrist by dropping a 0.5kg weight from eye height, to elicit the stretch reflex. At the beginning of the condition, the participant was asked to rotate the arm at the elbow to one of the positions. Participant was then asked to close his eyes and co-contract the biceps and triceps to the required level. The perturbation was then applied randomly in the next 5-20s to avoid prediction of impact. In addition, we recorded a third experiment which was used for validation purposes. In this experiment, "Loaded Reflex" (LR), we loaded the wrist with 1, 2, 3, 4 and 5kg weights and tested the reflex in a manner similar to the CR experiment. Before data collection, the participant was familiarized with the protocol and Maximum Voluntary Contraction (MVC) data were recorded for the post-processing stage.

A. Neuromusculoskeletal reference values

Musculoskeletal inverse kinematics and inverse dynamics were calculated using the sDIMS software [1]. Muscle tensions were computed by solving an optimization problem by quadratic programming. The constraints for this optimization come from the muscle forces estimated from EMG recordings, terms to minimize overall muscle force, and terms to ensure continuity of estimated values. The details of the musculoskeletal inverse dynamics algorithm can be found in [1]. External contact forces such as that exerted upon the force sensor in the GR experiment, or, the impact force of the falling weight in the CR experiment were applied to the wrist joint of the MS model. For the GR experiment, exerted force could be directly obtained from the force sensor readings. For the CR experiment, we estimated impact force using the recorded weight of the object and post-hoc analysis of the velocity profile. The output of the musculoskeletal analysis of the experimental data, and recorded EMG data, were used as reference for parameter identification. The references for the GR and CR experiments were:

$$x_{GR} = \begin{bmatrix} q & \tau & F_B & F_T & a_B & a_T \end{bmatrix}^T \quad (6)$$

$$x_{CR} = \begin{bmatrix} q(t) & \tau(t) & F_B(t) & F_T(t) & a_B(t) & a_T(t) \end{bmatrix}^T \quad (7)$$

where, q was the joint angle, τ the joint torque, F_B, F_T the bicep and tricep muscle forces, and a_B, a_T the corresponding muscle activations. Note that these were average values of the parameters over the duration of each GR condition (10s). The reference in eq. (6) was calculated for each of the 11 GR recruitment conditions. Note that for the CR experiment (6), the calculated reference vectors were for the 9 combinations of arm position and co-contraction level with, t=0-125ms. The reference period was chosen to be 25ms before, to 100ms after, the applied perturbation.

IV. PARAMETER IDENTIFICATION

We decomposed the identification process of the unknown model parameters into two stages; Steady-State, and, Dynamic. Steady-state parameters were identified by solving the least-squares objective function:

$$min \sum_{k=1}^{11} ||W(x_{GR} - \hat{x}_{GR})||^2 \quad (8)$$

$$\text{with, } \hat{x}_{GR} = [\hat{q} \quad \hat{\tau} \quad \hat{F}_B \quad \hat{F}_T \quad \hat{a}_B \quad \hat{a}_T]^T$$

$$f_{GR} = [C_{B\_SF} \quad C_{T\_SF} \quad Fmax_{B\_SF} \quad Fmax_{T\_SF}]$$

where, $k = 1..11$ refers to the conditions of the GR experiment. x_{GR} was the vector of reference values from eq. (6) and $\hat{x}_{GR}$ the steady state estimates from the forward dynamics simulation. W was a diagonal matrix of normalizing factors that adjusted the variables to the same order of magnitude.

These normalizing factors were determined post-hoc as the mean of the reference values x_{GR}. f_{GR} refers to the steady-state parameters to be identified. Eq. (8) was solved using the Limited memory BFGS-B algorithm coupled with a backtracking line search, subject to the bounds for free parameters f_{GR} specified in Table II-A. Dynamic parameters were identified similarly. To account for a trajectory of reference values (eq. (7)), we modified the problem as follows:

$$min \sum_{k=1}^{9} ||W \sum_{t=0}^{125} (x_{CR}(t) - \hat{x}_{CR}(t))||^2 \quad (9)$$

$$\text{with, } \hat{x}_{CR} = [\hat{q}(t) \quad \hat{\tau}(t) \quad \hat{F}_B(t) \quad \hat{F}_T(t) \quad \hat{a}_B(t) \quad \hat{a}_T(t)]^T$$

$$f_{CR} = \begin{matrix} [Tmax_{B\_SF} & Tmax_{T\_SF} & \tau_{SF} & w_{BB+} & .. \\ \sigma_{BB+} & w_{TT+} & \sigma_{TT+} & w_{BI+} & .. \\ \sigma_{BI+} & w_{IT-} & \sigma_{IT-}] & & \end{matrix}$$

where, $k = 1..9$, refers to the 3×3 conditions of the CR experiment. Here, the objective function (9) minimizes the error between forward dynamics estimate, $\hat{x}_{CR}$ and the reference x_{CR}, for t=0 to 125ms (impact at 25ms), with the free model parameters f_{CR} subject to the bounds in Table II-A.

A. Forward Dynamics Simulation and Identification

For fixed nominal control inputs (stimulation), we calculated neural spikes and subsequent muscle activation as detailed in Section II-A. From this activation, muscle tensions were calculated as detailed in Section II-B. Muscle tensions were transformed into equivalent joint torques and the resulting joint accelerations computed using the Runge-Kutta RK4 method. Two types of external forces were applied to the wrist joint of the model. For comparison with the GR experiment we applied a constant force equivalent to that exerted by the arm on the force sensor. For comparison with the CR experiment, we used the same impact force profile of the falling object, as that used in the inverse dynamics computation. Dynamics were computed every 0.5ms, with all trials lasting 6s. The identification process was implemented using the Python programming language, the Scipy Minimization Toolbox, and the MPI parallel processing environment. For steady-state parameter identification, we computed the cost (eq. (8)) for 1000 random combinations for the parameters in f_{GR} within the bounds defined in Table II-A. For f_{GR} combinations with the 10 lowest costs, we applied the L-BFGS-B minimization algorithm. Each minimization run took about 1 hour on a 18 $\times$ 3.1GHz workstation. Fig. 2-a shows the goodness of fit between the identified steady-state model results and the reference values. Dynamic parameter identification followed the same process as above for the parameters in f_{CR}. The complete identified model parameters are listed in the rightmost column of Table II-A.

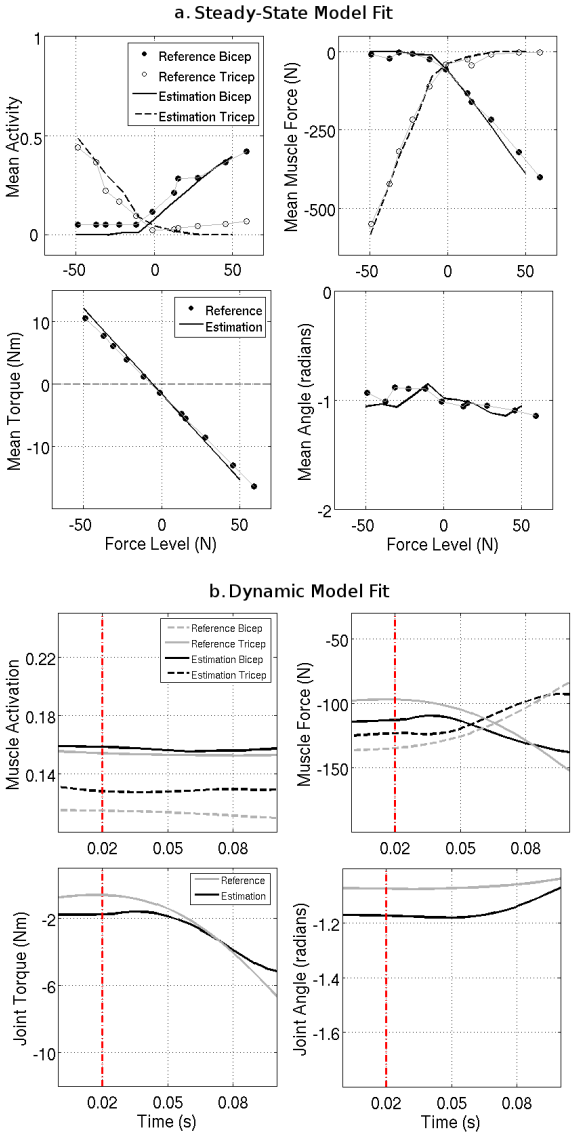

Fig. 2. (a) Steady-State Parameter Identification Results: Fit of forward dynamics model steady-state results, with the data from GR experiments. (b) Dynamic Parameter Identification Results: Fit of forward dynamics model dynamic results, with the data from CR experiment, for the condition [Arm Horizontal-Low Co-contraction]. Vertical dash-dot line indicates start of perturbation.

V. SIMULATION OF STRETCH REFLEX

Robustness of the identified model was tested by comparing it to the results obtained from the "Loaded Reflex" (LR) experiment. Note that the LR experiment was not used in the parameter identification process. LR data were processed in a similar manner to that of GR and CR experiments. For the complete model identified in Section IV-A we defined control inputs such that joint angles roughly matched those recorded during the LR experiment. We then applied identical loading force and perturbation to the forward dynamics model as that in the LR experiment. Fig. 3 shows the comparison for one condition (5kg loading) between LR reference values, and the estimated forward dynamics of the identified model. We observed that the forward dynamics simulation of the identified model was able to reproduce the LR experimental results. The differences between model and observed results were (median $\pm$ variance): 11.1 $\pm$ 2.8N for muscle forces, 0.04 $\pm$ 0.03 radians for joint angle, 0.16 $\pm$ 0.08Nm for joint torque and 0.03 $\pm$ 0.005 for muscle activations.

VI. DISCUSSION

This study proposes a model of the physiological stretch reflex arising from the interaction between a realistic spiking neural network and a musculoskeletal model. Although detailed modeling of neural control mechanisms add to the complexity of the overall system, it is likely that the benefits from such architectures will outweigh the drawbacks. This view is especially supported by looking at the state-of-the-art in complex machines that can provide human support/augmentation such as neuroprostheses and exoskeletons. From a human movement modeling perspective, the bio-mimetic model architecture and parameter identification from experimental data constrained within biological bounds, resulted in a identified model that could predict reflex characteristics beyond its training dataset, Fig. 3. We note that for a different posture the synaptic weights identified here may no longer be valid (for example, if we tested the tricep reflex instead of the bicep). Additionally, we are limited to an agonist-antagonist architecture which ignores possible effects from other interacting muscles (for example, the brachialis muscle in the upper arm). In this particular case (elbow flexion/extension), the role of the brachialis is minimal as it is mostly used for elbow torsion and multi-jointed movements. However, interacting muscles (and their corresponding neural pools) will have to be taken into account if we wish to model more elaborate movements. In the human CNS, this is organized by complex circuits of upper motor neurons and higher brain centers, which selective change the synaptic weights and pathways by inhibiting some while preferring others. One way to account for this is by extending our current architecture and implementing switching commands that mimic the higher control centers of the human CNS, for example like those used in [8], [7]. A limitation in our approach was that the overall response of the NMS model was significantly nonlinear and included muscular and reflexive components. Separating these influences can be quite difficult as neural dynamics are difficult to directly observe. Studies have proposed methods to overcome this limitation by linearizing the system and simplifying the reflex gains [4]. Under certain physiological conditions this linearization can be an appropriate strategy, however, effective identification techniques of nonlinear muscular and reflexive components for NMS models remains an open challenge.

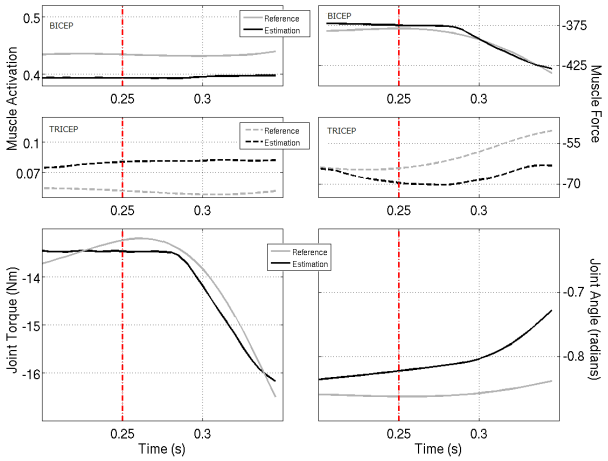

Fig. 3. Comparison plot between results from the identified model and the "Loaded Reflex" experiment

ACKNOWLEDGMENT

This research was supported by HPCI STRATEGIC PROGRAM Computational Life Science and Application in Drug Discovery and Medical Development by MEXT, Japan. The Authors would like to acknowledge Matthew Howard, Koh Ayusawa and Yosuke Ikegami for assistance with the experiments, software implementation and helpful discussions.

REFERENCES

[1] Y. Nakamura, K. Yamane, Y. Fujita, and I. Suzuki, "Somatosensory computation for man-machine interface from motion-capture data and musculoskeletal human model," *IEEE Tran. Robot.*, vol. 21, no. 1, 2005.

[2] A. Seth and M. G. Pandy, "A neuromusculoskeletal tracking method for estimating individual muscle forces in human movement," *J. Biomech.*, vol. 40, pp. 356–366, 2007.

[3] R. R. L. Cisi and A. F. Kohn, "Simulation system of spinal cord motor nuclei and associated nerves and muscles, in a web-based architecture," *J. Comp. Neurosci.*, vol. 25, pp. 520–542, 2008.

[4] A. C. Schouten, E. de Vlugt, J. B. van Hilten, and F. C. van der Helm, "Quantifying proprioceptive reflex during position control of the human arm," *IEEE Tran. Biomed. Engg.*, vol. 55, no. 1, pp. 311–321, 2008.

[5] K. Doya, "Complementary roles of the basal ganglia and cerebellum in learning and motor control," *Curr. Opin. Neurobiol.*, vol. 10, pp. 732–739, 2000.

[6] K. Hirasawa, K. Ayusawa, and Y. Nakamura, "Muscle activity estimation based on inverse dynamics and muscle stress analysis by finite element method," in *Proc. 19th CISM-IFToMM Symp. Robot Design, Dynamics, and Control*, 2012.

[7] H. Geyer and H. Herr, "A muscle reflex model that encodes principles of legged mechanics and produces human walking dynamics and muscle activities," *IEEE Tran. Neural Sys. Rehabil. Engg.*, vol. 18, no. 3, pp. 263–273, 2010.

[8] A. Murai, K. Yamane, and Y. Nakamura, "Modeling and identification of human neuromusculoskeletal network based on biomechanical property of muscle," in *Proc. IEEE Int. Conf. Engg. Med. Biol. Sci.*, 2008, pp. 3706–3709.

[9] E. Kandel, J. Schwartz, and T. Jessell, *Principles of Neural Science*. 4th ed. McGraw-Hill, New York, 2000.

[10] M.-O. Gewaltig and M. Diesmann, "Nest (neural simulation tool)," *Scholarpedia*, vol. 2, no. 4, p. 1430, 2007.

[11] M. Djurfeldt, J. Hjorth, J. Eppler, N. Dudani, M. Helias, T. Potjans, U. Bhalla, M. Diesmann, J. Kotaleski, and O. Ekeberg, "Run-time interoperability between neuronal network simulators based on the music framework," *Neuroinformatics*, vol. 8, no. 1, pp. 58–66, 2010.

[12] A. J. McComas, V. Galea, and H. de Bruin, "Motor unit populations in healthy and diseased muscles," *Physical Therapy*, vol. 73, pp. 868–877, 1993.

[13] D. Thurbon, H.-R. Luscher, T. Hofstetter, and S. Redman, "Passive electrical properties of ventral horn neurons in rat spinal cord slices," *J. Neurophysiol.*, vol. 79, pp. 2485–2502, 1998.

[14] A. Morrison, S. Straube, H. Plesser, and M. Diesmann, "Exact subthreshold integration with continuous spike times in discrete time neural network simulations," *Neural Comp.*, vol. 19, pp. 47–79, 2007.

[15] A. J. Fuglevand, D. Winter, and A. E. Patla, "Models of recruitment and rate coding organization in motor-unit pools," *J. Neurophysiol.*, vol. 70, pp. 2470–2488, 1993.

[16] A. Prochazka and M. Grassini, "Models of ensemble firing of muscle spindle afferents recorded during normal locomotion in cats," *J. Physiol.*, vol. 507.1, pp. 277–291, 1998.

[17] R. W. Banks, "An allometric analysis of the number of muscle spindles in mammalian skeletal muscles," *J. Anat.*, vol. 208, pp. 753–768, 2006.